J. Fluid Mech. (1988), *vol.* 192, *pp.* 287–312
Printed in Great Britain

Dissipative effects on the resonant flow of a stratified fluid over topography

By N. F. SMYTH

Department of Mathematics, University of Wollongong, P.O. Box 1144, Wollongong, NSW, 2500, Australia

(Received 28 August 1986 and in revised form 25 November 1987)

The effect of dissipation on the flow of a stratified fluid over topography is considered in the weakly nonlinear, long-wave limit for the case when the flow is near resonance, i.e. the basic flow speed is close to a linear long-wave speed for one of the long-wave modes. The two types of dissipation considered are the dissipation due to viscosity acting in boundary layers and/or interfaces and the dissipation due to viscosity acting in the fluid as a whole. The effect of changing bottom topography on the flow produced by a force moving at a resonant velocity is also considered. In this case, the resonant condition is that the force velocity is close to a linear long-wave velocity for one of the long-wave modes. It is found that in most cases, these extra effects result in the formation of a steady state, in contrast to the flow without these effects, which remains unsteady for all time. The flow resulting under the action of boundary-layer dissipation is compared with recent experimental results.

1. Introduction

The flow of a homogeneous or stratified fluid over topography for the case when the imposed upstream flow velocity is near a linear long-wave velocity for the fluid, this flow being referred to as resonant, has been the subject of much theoretical and experimental attention. The equation governing this flow in the long-wavelength, weakly nonlinear limit has been derived by Akylas (1984) and Cole (1985) for the case of a surface-pressure forcing whose lengthscale is much less than the characteristic lengthscale of the flow, by Lee (1985) for a general lengthscale surface pressure or topographic forcing and by Grimshaw & Smyth (1986) (hereinafter referred to as GS) for a general lengthscale topographic forcing in a stratified fluid. This equation is a forced Korteweg–de Vries equation, which can be written in the form

$$-A_t - \Delta A_x + 6AA_x + A_{xxx} + G_x(x) = 0 \tag{1.1}$$

when there are no dissipative effects or, for the case of a moving forcing, the undisturbed depth of the fluid is constant. The coordinate x is positive in the direction of the imposed upstream flow. The parameter Δ in (1.1) is a detuning parameter measuring how close the flow is to linear resonance, with $\Delta = 0$ corresponding to exact linear resonance; that is, the imposed upstream flow velocity equals a linear long-wave velocity. The function $G(x)$ is related to the form of the forcing.

Numerical solutions of (1.1) for various forms of the localized forcing G have been obtained by Akylas (1984), Cole (1985), Lee (1985) and GS. The form of these solutions was found to depend markedly on the sign of G. Positive forcing ($G > 0$) corresponds to the forcing and the soliton solutions of (1.1) having the same polarity,

and negative forcing ($G < 0$), the opposite polarity. For positive forcing, it was found that the flow upstream of the forcing consisted essentially of a train of solitons. Downstream of the forcing, a flat depression formed, followed by a modulated cnoidal wavetrain which brought the disturbance back to zero. The depression behind the forcing formed to compensate for the mass sent upstream. This solution is shown in figure 1(*a*). The parameters g_0 and ξ, the height and lengthscale of the forcing respectively, are formally defined in § 2. The salient feature of this flow is that no steady state forms upstream of the forcing; solitons are periodically generated at the forcing and sent upstream. For negative forcing, the solution is more complicated. This solution is shown in figure 1(*b*). The flow over the forcing remains unsteady, with modulated cnoidal waves sent downstream and isolated solitons sent upstream, with the period between these solitons being large. As explained by GS, the solution over the forcing remains unsteady as negative forcing acts to keep disturbances over the forcing.

GS obtained analytical approximations to the solution for positive forcing by assuming that upstream of the forcing, there exists a train of equal-amplitude, equally spaced solitons. The amplitude and spacing of these solitons was then found by using a mass and energy conservation argument. The downstream solution was obtained as a simple wave solution of the modulation equations for the Korteweg–de Vries equation, which were derived by Whitham (1974, §§ 16.14–16.16). These equations apply in the present context as the forcing is localized and hence the term G_x in (1.1) is effectively non-zero only in some finite region. The downstream solution agreed well with the numerical solution over the whole range of Δ. The agreement with the upstream numerical solution was good for Δ near zero, but for Δ away from zero, the agreement was not so good. Solutions agreeing with the numerical solutions over the whole range of Δ (in the resonant regime, which will be defined in the next paragraph) were obtained by Smyth (1987) as simple wave solutions of the modulation equations for the Korteweg–de Vries equation. In this solution, the upstream solution was found as a modulated cnoidal wave with modulus squared ranging from 1 at the front of the wavetrain to some value $m_0, 0 \leqslant m_0 < 1$ at the forcing. For Δ near zero, m_0 was close to 1, so that the upstream solution is essentially a train of solitons.

It was found by GS and Smyth (1987) that the resonant solution exists only for some resonant band $\Delta_1 < \Delta < \Delta_2$ of Δ, where $\Delta_1 < 0, \Delta_2 > 0$ and Δ_1 and Δ_2 depend on the forcing. Outside this band, the solution is qualitatively the same as the linear, non-resonant solution. For a broad forcing, which is the focus of the present work, it was found that $\Delta_1 = -\frac{1}{2}(12g_0)^{\frac{1}{2}}$ and $\Delta_2 = (12g_0)^{\frac{1}{2}}$, g_0 being the amplitude of G. In the analytical solutions of GS and Smyth, the net effect of the forcing is to produce a jump down in the mean level of the flow as the forcing is crossed. For a broad forcing, GS showed that the mean value of A just upstream of the forcing is given by

$$A_- = \tfrac{1}{6}[\Delta + (12g_0)^{\frac{1}{2}}], \tag{1.2}$$

and the mean value of A just downstream of the forcing is

$$A_+ = \tfrac{1}{6}[\Delta - (12g_0)^{\frac{1}{2}}]. \tag{1.3}$$

In the numerical and analytical solutions described above, the fluid was assumed to be inviscid and of uniform initial depth away from the forcing. In experimental and observational situations, viscous forces, and, for a moving forcing, changes in the undisturbed depth of the fluid, are present and these may result in significant alterations to the analytical solutions of GS and Smyth (1987). This is especially so

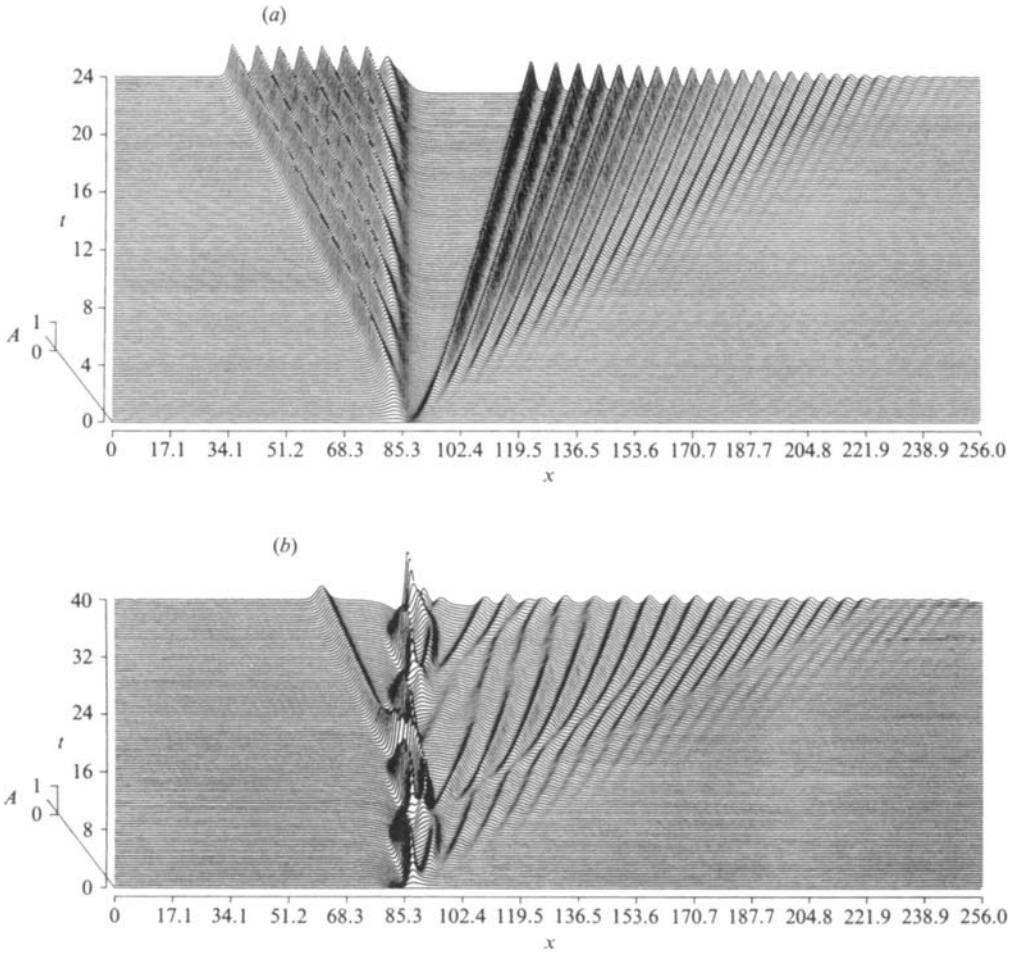

FIGURE 1. Numerical solution for forcing (2.6*a*) with $\xi = 0.3, \Delta = 0$ and no dissipation. (*a*) $g_0 = 1$, (*b*) -1.

in the resonant flow regime as, for positive forcing, it is predicted that the flow upstream of the forcing remains unsteady with waves continually being generated at the forcing and sent upstream. The effect of viscosity (and depth changes) on this predicted flow is of importance in determining the significance of the analytical solution to experimental and observational situations and to the question of whether a steady state will ultimately be formed. The resonant flow can be produced in experimental situations (Baines 1984; Lee 1985; Melville & Helfrich 1987); however, viscosity and depth changes could affect the occurrence of this flow in oceanographic and meteorological situations. Furthermore, the predicted flow for negative forcing is highly unsteady (see figure 1*b*) and it is expected that viscosity will have a marked effect on this flow. Determining the effect of viscosity on the flow for negative forcing will indicate how readily this flow can be produced experimentally (the author knows of no experiments or observations corresponding to negative forcing in the resonant regime).

In the present work, three effects will be considered; these being (1) changes in fluid depth, (2) the action of viscosity in boundary layers and/or interfaces and (3)

the action of viscosity in the fluid as a whole. Case (2) is of most importance in experimental situations, with the other two cases being of importance for oceanographic and meteorological situations. Case (1) is of relevance only for the situation of a moving forcing (e.g. a pressure distribution). The equation governing the resonant flow under one of the additional effects (1)–(3) is the forced Korteweg–de Vries equation (1.1) with an appropriate additional term. The form of these additional terms is discussed in the next section, with the detailed discussion of the equations appearing in §§3–5. It is found that viscosity causes the predicted upstream and downstream wavetrains for positive forcing to eventually become undular bores. Viscous effects are found to go some way towards explaining the difference between the experimental results of Lee (1985) and Melville & Helfrich (1987) and the inviscid theoretical predictions, although this is complicated by the fact that higher-order nonlinear and dispersive terms also have an effect. Interest centres on the effects of (1)–(3) on the resonant solution. The effects on the non-resonant solution (i.e. that for $\Delta > \Delta_2$ or $\Delta < \Delta_1$) are not considered here, as no major changes are introduced and the non-resonant solution behaves in the expected manner.

2. Forced Korteweg–de Vries equations incorporating viscosity and depth changes

Let us consider the two-dimensional flow of a stratified fluid over localized topography. To describe the flow, a horizontal coordinate X, a vertical coordinate z and a time T are used, where these coordinates have been non-dimensionalized by a lengthscale h_1, h_1 being a typical vertical dimension and a timescale N_1^{-1}, N_1 being a typical value of the Brunt–Väisälä frequency. We assume that the basic flow state has a constant horizontal velocity of magnitude V in the direction of X, a non-dimensional density $\rho_0(z)$ (non-dimensionalized by a typical density) and a non-dimensional pressure $p_0(z)$, where $p_{0z} = -\rho_0$. The topography is given by

$$z = -h + \alpha g(\beta X), \tag{2.1}$$

where $\alpha = a/L, \beta = h_1/L$, a being a typical amplitude of the topography and L a typical horizontal lengthscale. Since the topography is assumed to be localized, so that $g \to 0$ as $X \to \pm\infty$, this defines the origin of z if h is defined to be the undisturbed depth of the fluid. This flow is considered in the weakly nonlinear, long-wave limit, so that $\alpha \ll 1, \beta \ll 1$. We further specialize to the particular case when the imposed upstream flow velocity is near a linear long-wave velocity for the fluid. In this situation, linear theory predicts a singular solution as energy cannot propagate away from the obstacle. As stated in the introduction, in the absence of dissipation, the equation describing the flow under these conditions is the forced Korteweg–de Vries equation

$$-A_t - \Delta A_x + 6AA_x + A_{xxx} + G_x = 0. \tag{2.2}$$

The initial condition to be used in the present work is

$$A(x, 0) = 0, \tag{2.3}$$

which corresponds to switching on the forcing at $t = 0$. This equation represents a balance between nonlinearity and dispersion, which, since the flow is resonant and produces a response of $O(\alpha^{\frac{1}{2}})$, requires $\beta^2 = \alpha^{\frac{1}{2}}$. The functions A and G, the detuning parameter Δ and the coordinates x and t are related to the physical vertical

displacement ζ, the physical bottom topography, the imposed upstream flow velocity and the physical horizontal space and time coordinates by

$$\left.\begin{aligned} t &= \lambda c_n \beta \alpha^{\frac{1}{2}} T, \\ x &= \beta X, \\ \zeta &= \alpha^{\frac{1}{2}} \frac{6\lambda}{\mu} A \phi_n(z), \\ V &= c_n(1+\alpha^{\frac{1}{2}}\lambda \Delta), \\ I_n G &= \frac{\mu}{12\lambda^2} \rho_0 c_n^2 \phi_{nz}(-h)\, g(\beta X), \end{aligned}\right\} \tag{2.4}$$

where

$$\begin{aligned} 2I_n \mu &= 3 \int_{-h}^{0} \rho_0 c_n^2 \phi_{nz}^3 \, \mathrm{d}z, \\ 2I_n \lambda &= \int_{-h}^{0} \rho_0 c_n^2 \phi_n^2 \, \mathrm{d}z, \\ I_n &= c_n^2 \int_{-h}^{0} \rho_0 \phi_{nz}^2 \, \mathrm{d}z, \end{aligned}$$

$\phi_n(z)$ being the modal function and c_n the linear phase speed for the resonantly forced long-wave mode (see GS).

It should be noted that in obtaining (2.2), it has been assumed that the scaled out coefficient μ of the nonlinear term is $O(1)$. This is not the case, for example, for a fluid with constant Brunt–Väisälä frequency and small Boussinesq parameter $h_1 N_1^2 g^{-1}$, in which case (2.2) is not a valid approximation and terms cubic in the amplitude must be included. As noted in the introduction, (2.2) also describes the flow produced by a moving two-dimensional force (such as a moving pressure distribution on the surface of a fluid of constant density) in the weakly nonlinear, long-wave limit when the velocity of the force is near a linear long-wave velocity. In this case, the forcing function G is given by an expression similar to that in (2.4) which involves this force (see Akylas 1984; Cole 1985; or Lee 1985).

In the present work, it is assumed that the forcing function G is of the form

$$\begin{aligned} G(x) &= g_0 G'(x'), \\ x' &= \xi x. \end{aligned} \tag{2.5}$$

The function G' is taken to have the following properties: $G'(x') \geqslant 0$ for all x', G' has a maximum value of 1 at $x' = 0$ and $G' \to 0$ as $x' \to \pm\infty$. The parameter ξ measures the lengthscale of the forcing. The forcing is therefore assumed to be localized and of one sign.

GS studied the initial-value problem (2.2) and (2.3) both analytically and numerically. The numerical solutions were obtained using the pseudospectral method of Fornberg & Whitham (1978) with the forcing functions

$$G = g_0 \operatorname{sech}^2 \xi x, \quad G = g_0 \mathrm{e}^{-\xi^2 x^2}. \tag{2.6a, b}$$

The numerical solution of (2.2) and (2.3) for $\Delta = 0$ and the forcing function (2.6a) with $g_0 = 1$ and $\xi = 0.3$ is shown in figure 1(a). In figure 1(b), the solution is shown for $\Delta = 0, g_0 = -1$ and $\xi = 0.3$. For convenience, the numerical solutions in this paper have the forcing function centred at $x = 85$. As discussed in the introduction, GS and Smyth (1987) obtained analytical approximations to the solution for positive forcing that were in good agreement with the numerical solutions. For further details of this non-dissipative solution, the reader is referred to this work.

The equations for resonant flow when viscosity and variable fluid depth are added are now discussed before their solutions are taken up in detail in §§ 3–5.

2.1. *Variable fluid depth*

The forced Korteweg–de Vries equation for a force moving near resonance in a fluid with variable undisturbed depth is

$$-A_s-\Delta A_\theta+6AA_\theta+A_{\theta\theta\theta}+G_\theta(\theta)=\Gamma(s)\,A, \tag{2.7}$$

where, from Grimshaw (1983),

$$\left.\begin{aligned}\Gamma(s)&=-\frac{(c_n^2I_n)_s}{2c_n^2I_n}-\frac{\mu}{\lambda^{\frac{1}{3}}}\left(\frac{\lambda^{\frac{1}{3}}}{\mu}\right)_s,\\ s&=\int_0^{\alpha x}\frac{\mathrm{d}\xi}{c_n(\xi)},\\ \theta&=\frac{\lambda^{-\frac{1}{3}}}{\alpha}(s-\alpha t),\end{aligned}\right\} \tag{2.8}$$

the subscript s denoting differentiation with respect to s. The physical coordinate x is related to s by (2.8*b*).

For the special case of a force moving on the surface of a fluid with constant density,

$$\Gamma(s)=\frac{9h_s}{4h}. \tag{2.9}$$

In § 3, the particular case

$$\Gamma=\epsilon, \tag{2.10}$$

$\epsilon>0$ a constant, is discussed. This choice of Γ has the advantage of simplicity as well as being representative of increasing depths. The depth change (2.10) acts as a damping, as can be seen upon consideration of the energy conservation equation for (2.7). The dispersion relation for the dispersive part of the unforced equation (2.7) with (2.10) is

$$\omega=\Delta k+k^3-\mathrm{i}\epsilon. \tag{2.11}$$

This depth change then has a uniform effect on all frequencies.

2.2. *Boundary-layer viscosity*

The equation incorporating the effect of viscosity in boundary layers and/or interfaces on the resonant flow of a fluid is

$$-A_t-\Delta A_x+6AA_x+A_{xxx}+G_x-\delta V(A)=0, \tag{2.12}$$

where

$$\left.\begin{aligned}V(A)&=\frac{1}{2\pi}\int_{-\infty}^{\infty}(-\mathrm{i}k)^{\frac{1}{2}}\,\mathrm{e}^{\mathrm{i}kx}F(A)\,\mathrm{d}k,\\ F(A)&=\int_{-\infty}^{\infty}\mathrm{e}^{-\mathrm{i}k\theta}A(\theta,t)\,\mathrm{d}\theta.\end{aligned}\right\} \tag{2.13}$$

Miles (1976) and Grimshaw (1983) showed that the Fourier transform/antitransform pair gives the effect of boundary-layer friction. This formulation of the effect of boundary-layer friction is equivalent to that originally given by Keulegan (1948). Physically and experimentally, this is generally the most important type of dissipation due to viscosity. The parameter δ is given by (see Grimshaw 1983)

$$I_n\,\delta=\left(\frac{\nu'}{\beta^5}\right)^{\frac{1}{2}}\frac{c_n}{\lambda}\left(1+\frac{2h}{b}\right)\phi_{nz}^2(-h), \tag{2.14}$$

where ν' is the non-dimensional kinematic viscosity (an inverse Reynolds number) and b is the non-dimensional breadth of the channel the motion takes place in. The second to last factor, incorporating the effect of any sidewalls ($b = \infty$ if there are none), was found by Hammack & Segur (1974) and Weidman & Maxworthy (1978) to improve agreement with experimental results. It can be seen that the parameter δ is proportional to the square root of the kinematic viscosity. For the special case of surface waves on a fluid of constant density

$$\delta = 6\left(\frac{\nu'}{\beta^5}\right)^{\frac{1}{2}}\left(1+\frac{2h}{b}\right), \tag{2.15a}$$

and for a two-layer fluid with lower-layer density ρ_2, upper-layer density ρ_1, lower-layer depth d and total depth h,

$$\delta = \left(\frac{\nu'}{\beta^5}\right)^{\frac{1}{2}} \frac{6\sqrt{2}\left(1+\frac{2h}{b}\right)(\rho_1 d+\rho_2(h-d))^{\frac{1}{2}}}{d^2[h(h-d)(\rho_1+\rho_2)]^{\frac{1}{2}}[\rho_2 d+\rho_1(h-d)]} \tag{2.15b}$$

(see Leone, Segur & Hammack 1982 and Grimshaw 1983). For the case of a two-layer fluid, the densities are non-dimensionalized by the mean density of the two fluids and the depths are non-dimensionalized by the product of the depths of the two layers divided by the total depth.

2.3. *Viscosity of the fluid as a whole*

The final additional process considered in the present work is that due to the kinematic viscosity of the fluid as a whole. The derivation of GS of the forced Korteweg–de Vries equation can be simply extended to include the viscous terms of the Navier–Stokes equations. This derivation is not given here as the extension is minor. The end result is that the forced Korteweg–de Vries equation including the effect of the viscosity of the fluid as a whole is

$$-A_t - \Delta A_x + 6AA_x + A_{xxx} + G_x + \nu A_{xx} = 0, \tag{2.16}$$

where ν is given by

$$I_n \nu = \frac{\nu' c_n}{2\beta\lambda}, \tag{2.17}$$

ν' being the non-dimensional kinematic viscosity of the fluid (inverse Reynolds number). For surface waves on a fluid of constant density,

$$\nu = \frac{3\nu'}{\beta}. \tag{2.18}$$

Equation (2.16) is a forced KdV–Burgers equation.

Which of the three effects (1)–(3) dominates in a given situation depends on the relationship between ϵ, δ and ν. In most physical and experimental situations, the dominant form of viscous decay is that of Case (2) (see § 1) as δ depends on the square root of the kinematic viscosity, whereas ν is proportional to the kinematic viscosity. Also, in experimental situations, the variation in the depth of the fluid is so small that $\epsilon \ll \delta$. The effect of the viscosity of the fluid as a whole is discussed as while both this form of viscous decay and boundary-layer viscosity lead to undular bores forming upstream and downstream of the forcing, the long-term behaviour in the two cases is different in that the bore for the viscous decay of (3) becomes steady, while that for the boundary-layer viscosity of (2) decays to zero.

The three equations (2.7), (2.12) and (2.16) are solved numerically using the pseudo-spectral method of Fornberg & Whitham (1978). The forcing

$$G = g_0 \operatorname{sech}^2 \xi x \tag{2.19}$$

is used as the solutions for this choice of G are representative of the class of forcings G with properties given by (2.5) (see GS). Furthermore, only the case of a broad forcing, so that ξ is small, is considered. This limit is chosen as it is the case of most geophysical significance and the overall features of the solution do not depend on the lengthscale of the forcing (see GS).

A preliminary idea of the relative effect of the two types of viscous dissipation may be obtained by considering the dispersion relations for the non-forced, dispersive parts of (2.12) and (2.16). These dispersion relations are

$$\omega = \Delta k + k^3 - \frac{\delta k^{\frac{1}{2}}}{\sqrt{2}}(1+\mathrm{i}) \tag{2.20}$$

and

$$\omega = \Delta k + k^3 - \mathrm{i}\nu k^2 \tag{2.21}$$

respectively. The higher frequencies for (2.16) are damped out faster than those for (2.12). The viscous damping of (2.12) can be thought of as weak and that of (2.16) as strong (for equal values of δ and ν). For both types of viscous dissipation, the higher wavenumbers are preferentially damped out. This is in contrast to the case for (1), where all wavenumbers are damped uniformly. It is therefore expected that the solutions for the two types of viscous decay will be similar and very different from those for (1). This expectation is borne out in the numerical solutions presented in the next three sections.

From the work of GS, it is expected that the solutions for positive and negative forcing will be of different form. Also, it is expected that the solutions for large and small values of the damping or bottom slope will be different. Therefore, the solutions for positive and negative forcing, with either small or large bottom slope or weak or strong damping, are discussed separately for each of (1)–(3).

3. Forced Korteweg–de Vries equation with changing fluid depth

In this section, the equation

$$-A_s - \Delta A_\theta + 6AA_\theta + A_{\theta\theta\theta} + G_\theta - \epsilon A = 0 \tag{3.1}$$

is considered, this equation giving the effect of a particular type of changing bottom topography on the flow produced by a resonantly moving forcing. It is anticipated from the work of GS that the solutions of (3.1) fall into two broad classes, namely those for positive and negative forcing. Let us first consider the case of positive forcing.

3.1. *Positive forcing, small bottom slope*

The numerical solutions of (3.1) with $\Delta = 0, \epsilon = 0.05, 0.15$ and the forcing (2.19) with $g_0 = 1$ and $\xi = 0.3$ are shown in figure 2 (*a* and *b*). For comparison, the solution for $\epsilon = 0$ is shown in figure 1 (*a*). The effect of increasing depth can be clearly seen. On the upstream side of the forcing, some of the waves are being overtaken by the wave behind. Waves produced at an earlier time are damped more since the damping has acted on them for a longer time. If this damping is large enough, a given wave will slow down sufficiently for the wave behind it to interact with and overtake it. This

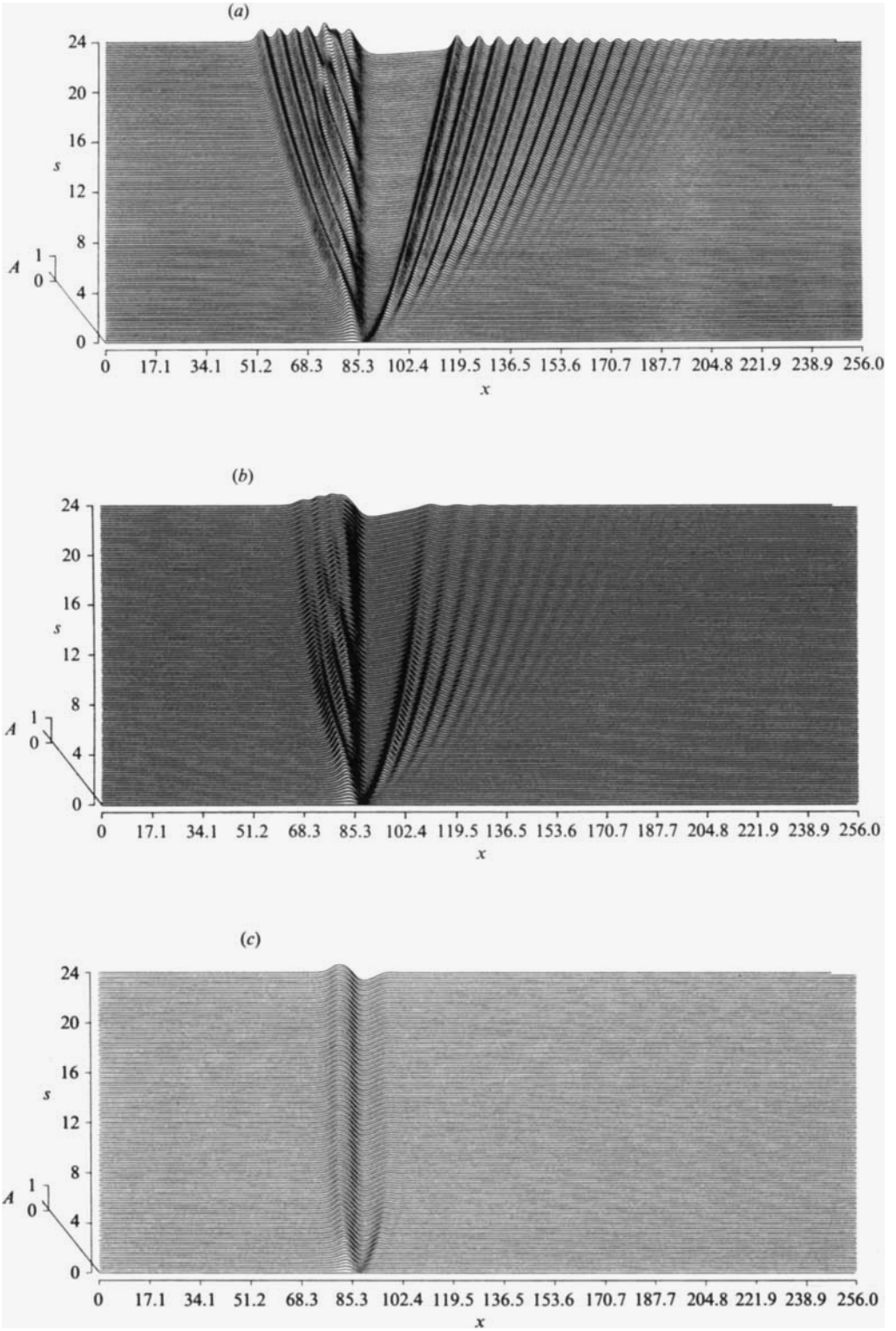

FIGURE 2. Numerical solution of (3.1) with $\Delta = 0, g_0 = 1, \xi = 0.3$. (*a*) $\epsilon = 0.05$, (*b*) 0.15, (*c*) 0.50.

	Numerical slope		Theoretical slope	
ϵ	Upstream	Downstream	Upstream	Downstream
0.05	—	−0.008	0.0083	−0.0083
0.10	~0.014	−0.016	0.0167	−0.0167
0.15	0.024	−0.025	0.0250	−0.0250

TABLE 1. Slopes of the long-term solution for ϵ small

overtaking is facilitated by the fact that solitons interact and overtake at a distance if their amplitudes are sufficiently similar. The solitons, in effect, are changing identity upon overtaking. As ϵ increases, these overtaking events occur more often due to the increased slowing down of the waves because of the greater damping.

It can be seen from figures 1 and 2 that the waves in the downstream modulated cnoidal wavetrain have slower phase speed and the downstream depression is of lesser extent and depth compared with the solution for $\epsilon = 0$. The reason for this can be seen from consideration of the expression for the phase speed of cnoidal waves. The phase speed of a cnoidal wave of mean height $\bar{A}$, amplitude a and modulus squared m is

$$c = \Delta - 6\bar{A} - 4a\left[\frac{2}{m} - 1 - \frac{3E}{mK}\right], \tag{3.2}$$

where E and K are complete elliptic integrals of the first and second kinds respectively. It can be seen that the phase speed of a cnoidal wave decreases as $\bar{A}$ and a increase. For the solutions shown in figure 2, the accelerating effect of the reduction in a is overcome by the deceleration due to the increase in $\bar{A}(\bar{A} < 0)$. Hence the modulated cnoidal wavetrain slows down and the downstream depression decreases in length.

From figure 2(*b*) in particular, it can be seen that the solution upstream of the forcing tends to a solution that decreases linearly to zero and that downstream of the forcing, the solution tends to one that increases linearly to zero. These linear portions are connected by a steady state over the forcing. The reason for this behaviour can be found upon consideration of (3.1). For $\Delta = 0$, this equation has the exact particular solution

$$A = \frac{\epsilon\theta}{6} + C \tag{3.3}$$

for $G = 0$, where C is a constant. The constants C_- for the upstream solution and C_+ for the downstream solution are obtained by matching with the steady state over the forcing. Corner layers need to be fitted where the linear portions near A equal to 0. In table 1, the theoretical slopes of these linear sections of the long-term solution are compared with the numerical slopes. There is no entered numerical value of the upstream slope for $\epsilon = 0.05$ as the upstream solution takes a long 'time' to evolve into a steady state and for $\epsilon = 0.05$, this 'time' was too large for a value of the upstream slope to be conveniently obtained. It can be seen that the agreement between the theoretical slopes given by (3.3) and the numerical slopes is quite good.

Small values of ϵ thus cause the solution of (3.1) for positive forcing to tend to a steady state as $s \to \infty$. For $\Delta = 0$, this steady state consists of a steady state over the forcing with linear sections upstream and downstream of the forcing, given by (3.3),

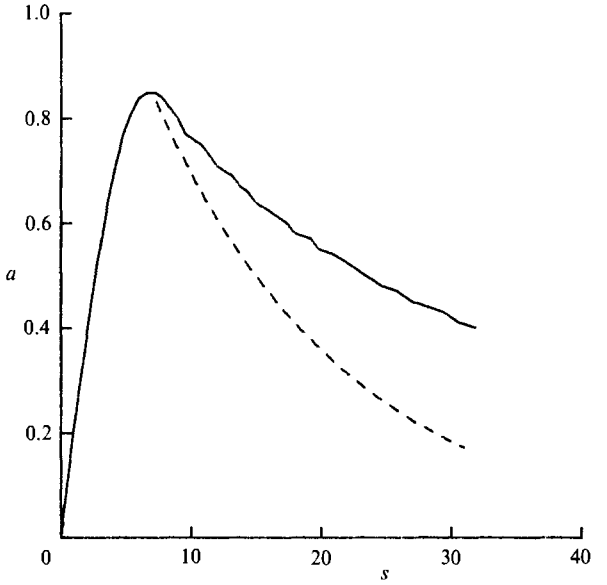

FIGURE 3. Amplitude a of the lead wave of the upstream wavetrain in figure 2(a) as a function of s (——); amplitude a of an unforced isolated soliton as a function of s (– – – –).

taking the solution to zero at a finite distance upstream and downstream. The behaviour of the solution for $\Delta \neq 0$ and Δ in the resonant band $-\frac{1}{2}(12g_0)^{\frac{1}{2}} < \Delta < (12g_0)^{\frac{1}{2}}$ will be similar. In particular, the steady flow outside of the forcing region will be the solution of

$$-\Delta A_\theta + 6AA_\theta + A_{\theta\theta\theta} - \epsilon A = 0. \tag{3.4}$$

Unfortunately, this equation cannot be solved exactly for $\Delta \neq 0$. For general bottom profiles (i.e. general $\Gamma(s)$), the long-term solution will be more complicated than that for $\Gamma = \epsilon$. For profiles with increasing depth, the solution away from the forcing will decay to zero and only a local solution about the forcing will remain. This is because a steady solution similar to (3.3) cannot form when Γ is not a constant. For a profile in which the depth decreases, the effect of Γ is to feed energy into the solution and the waves grow in amplitude rather than decay as in figure 2(a, b). This will ultimately result in the waves breaking in a physical situation. Of course, the weakly nonlinear assumption used in deriving the forced Korteweg–de Vries equation ceases to be valid before breaking.

Since the theoretical upstream wavetrain of Smyth (1987) for Δ near zero and $\epsilon = 0$ is nearly a train of solitons, it might be expected that the behaviour of the wavetrain for $\epsilon \neq 0$ will be given by the behaviour of a single soliton in variable-depth fluid. This is not the case however as the upstream wavetrain is actually a modulated cnoidal wavetrain whose individual waves are linked together and, through this linkage, to the forcing. While it is sufficient to consider the upstream wavetrain as a series of solitons for qualitative purposes, this is not so for any quantitative analysis, in which case the full modulated cnoidal wave character must be invoked. Knickerbocker & Newell (1980) showed the amplitude a of the soliton solution of (3.1) for $G = 0$ decays as

$$a = a_0 \, \mathrm{e}^{-\frac{4}{3}\epsilon(s-s_0)}, \tag{3.5}$$

where a_0 is the initial amplitude and s_0 the 'initial time' of the soliton. In figure 3, the amplitude a of the lead wave of figure 2(*a*) is plotted as a function of s. Also plotted is the amplitude decay (3.5) of a single unforced soliton. The initial amplitude a_0 of this soliton was chosen to be the maximum amplitude reached by the lead upstream wave of figure 2(*a*) and the 'initial time' s_0 was chosen to be the value of s at which this maximum is attained. As the initial period of amplitude growth is dominated by the effect of the forcing and occurs over a relatively small interval of s, the effect of changing bottom topography will be relatively minor over this amplitude growth period for small ϵ and this choice for a_0 and s_0 will be reasonable. It can be seen that the amplitude behaviour of the lead wave is very different from the amplitude behaviour of an isolated, unforced soliton. This is due to the upstream wavetrain being a modulated cnoidal wave, not a series of totally isolated solitons. If this wavetrain were a series of isolated solitons, (3.5) shows that these waves would all individually decay to zero and the steady state seen developing in figure 2(*a*) could not occur. It is the linkage between the individual waves of the upstream wavetrain and the linkage of the wavetrain to the forcing which allows this steady state to develop. Ovstrovsky (1976) showed that as a cnoidal wave solution of (3.1) for $G = 0$ decays, its modulus decreases. Therefore as s increases, the upstream wavetrain will become less and less like a train of solitons and its behaviour will increasingly diverge from (3.5), which can be seen occurring in figure 3. The detailed behaviour of the upstream wavetrain will not be given by the results of Ovstrovsky however, as his results apply to a wavetrain of a single modulus and, furthermore, the upstream wavetrain is linked to the forcing.

3.2. *Positive forcing, large bottom slope*

The effect of large bottom slope is shown in figure 2(*c*), where the solution of (3.1) is shown for $\Delta = 0, g_0 = 1, \xi = 0.3$ and $\epsilon = 0.5$. The solution in this case is a steady state over the forcing. This steady state is due to a balance between the forcing and the dissipation and hence is basically the solution of

$$G_\theta = \epsilon A, \tag{3.6}$$

so that

$$A = \frac{G_\theta}{\epsilon}. \tag{3.7}$$

Large bottom slope completely annihilates the upstream and downstream modulated cnoidal wavetrains of the solution for constant fluid depth and leaves only a local steady state in the neighbourhood of the forcing.

3.3. *Negative forcing, small bottom slope*

The effect of small bottom slope on the solution for negative forcing is shown in figure 4(*a*) where the solution for $\Delta = 0, g_0 = -1, \xi = 0.3$ and $\epsilon = 0.05$ is shown. For comparison, the solution for $\epsilon = 0$ is shown in figure 1(*b*). The damping $\epsilon = 0.05$ is sufficiently large to stop any waves from being sent upstream and to damp out most of the downstream wavetrain. The solution near the forcing remains unsteady; however the amplitudes of the waves near the forcing have been greatly reduced from those for $\epsilon = 0$.

3.4. *Negative forcing, large bottom slope*

An example of the solution for negative forcing and large bottom slope is shown in figure 4(*b*), where the numerical solution of (3.1) is shown for $\Delta = 0, g_0 = -1, \xi = 0.3$

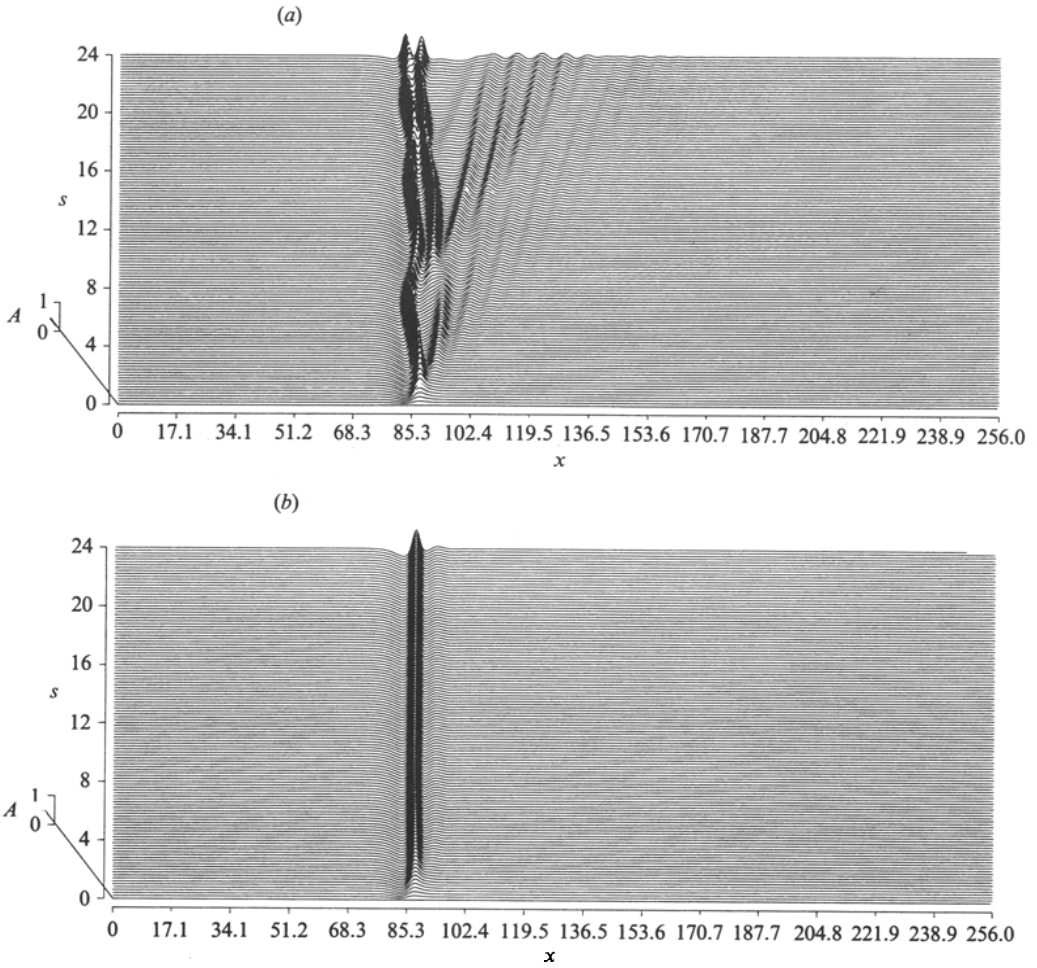

FIGURE 4. Numerical solution of (3.1) with $\Delta = 0$, $g_0 = -1$ and $\xi = 0.3$. (*a*) $\epsilon = 0.05$, (*b*) 0.50.

and $\epsilon = 0.5$. It can be seen that a large bottom slope leads to a localized steady state at the forcing, again resulting basically from a balance between the dissipation and the forcing.

Large values of ϵ, corresponding to rapidly increasing fluid depth, have physical significance, while large values of δ and ν, to be discussed in the next sections, have less physical significance as they correspond to Reynolds numbers much smaller than those usually encountered. We see that rapid changes in the fluid depth result in flows that are completely different to those for uniform fluid depth. The flow for large ϵ is limited to the region of the forcing.

4. Forced Korteweg–de Vries equation with boundary-layer friction

The next type of dissipation to be considered in the present work is that due to the action of viscosity in boundary layers and/or interfaces. As explained in §2, the equation describing the effect of boundary-layer viscosity on resonant flow is

$$-A_t - \Delta A_x + 6AA_x + A_{xxx} + G_x - \delta V(A) = 0. \tag{4.1}$$

Let us first consider the case of positive forcing.

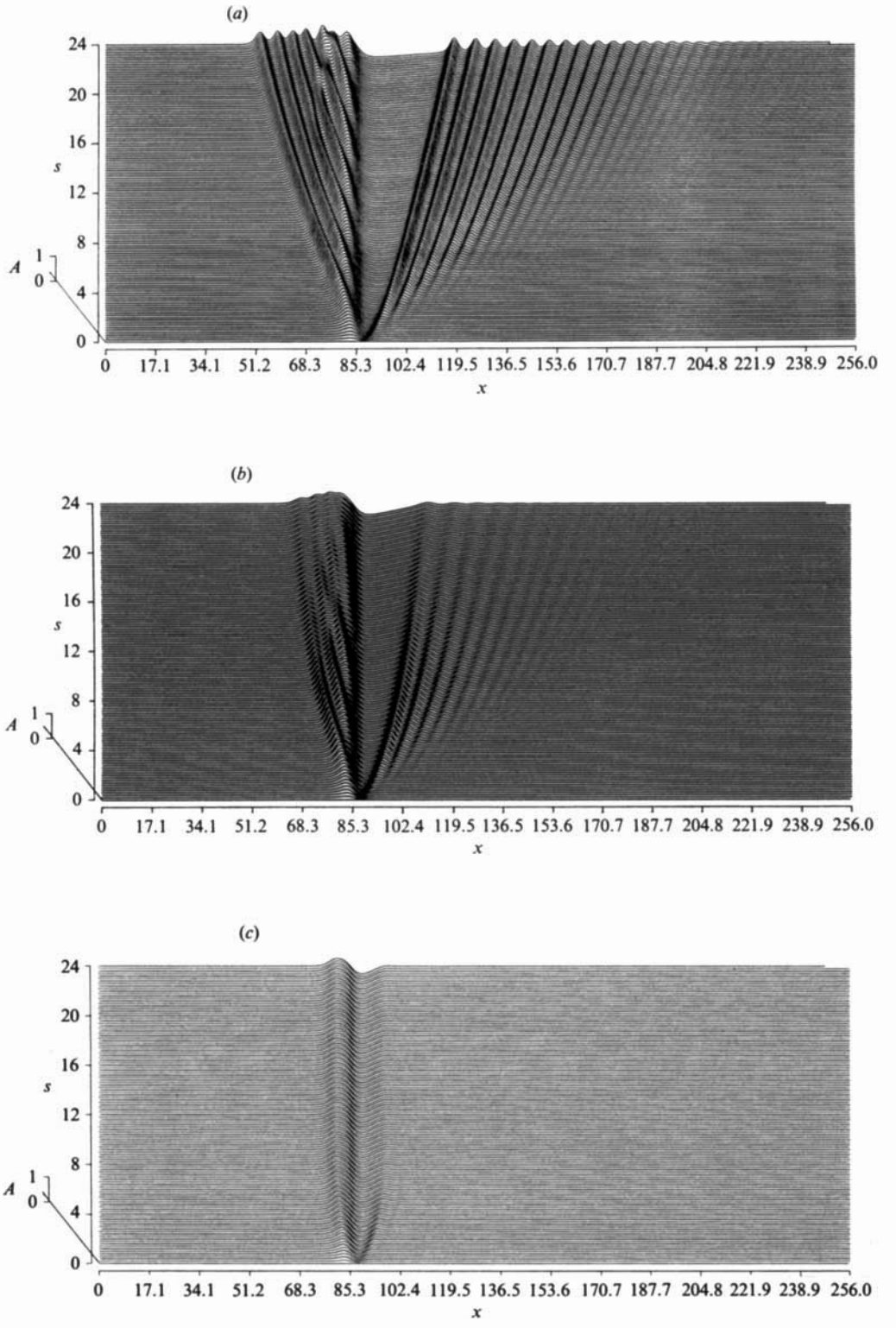

FIGURE 5. Numerical solution of (4.1) with $\Delta = 0$, $g_0 = 1$ and $\xi = 0.3$. (*a*) $\delta = 0.1$, (*b*) 0.3, (*c*) 1.0.

4.1. *Positive forcing, weak damping*

The numerical solutions of (4.1) for $\Delta = 0, \delta = 0.1, 0.3$ and the forcing (2.19) with $g_0 = 1$ and $\xi = 0.3$ are shown in figure 5 (a, b). For comparison, the numerical solution for $\delta = 0$ is shown in figure 1 (a). It can be seen that the solutions for weak boundary-layer viscosity and changing bottom profile are quite different. Weak boundary-layer viscosity results in the formation of an unsteady undular bore upstream of the forcing. A bore is a smooth jump between two different levels and thus a constant must be a solution of the equations governing the bore so that these two different levels are locally solutions. Therefore since a constant is a solution of (4.1), but not of (3.1), equation (4.1) can possess an undular bore solution, while (3.1) cannot. This difference in the solutions was anticipated on the basis of the spectral behaviour of the two types of damping, as discussed in §2.

Johnson (1970) showed that the unforced KdV–Burgers' equation has a steady undular bore as a solution. It is now shown that the unforced equation (4.1) does not possess a similar solution. As in Johnson, let us suppose that (4.1) has a steady undular bore of velocity U as a solution and that the jump across this bore is A_∞. This steady bore is then the solution of

$$(U-\Delta)A_x + 6AA_x + A_{xxx} - \delta V(A) = 0. \tag{4.2}$$

A multiple-scales solution of the form

$$A = A_0(\theta, \tau) + \delta A_1(\theta, \tau) + \ldots \tag{4.3}$$

is sought for this equation, where

$$\left.\begin{aligned} \theta &= \tfrac{1}{2}(3A_\infty)^{\frac{1}{2}}[x + (3A_\infty - \Delta)t] \\ \text{and} \qquad \tau &= \delta[x + (3A_\infty - \Delta)t]. \end{aligned}\right\} \tag{4.4}$$

At first order, it is found that

$$\left.\begin{aligned} A_0 &= b(\tau) + a(\tau)\,\mathrm{cn}^2\,\alpha(\tau)\,\theta, \\ b = \tfrac{1}{2}A_\infty - \frac{a}{3m}(2m-1), \quad a &= \tfrac{3}{2}A_\infty\, m(m^2-m+1)^{-\frac{1}{2}}, \\ \alpha = \left(\frac{2a}{3m}\right)^{\frac{1}{2}}, \quad U &= \Delta - 3A_\infty. \end{aligned}\right\} \tag{4.5}$$

At $O(\delta)$, we find the orthogonality relations

$$\oint V(A_0)\,\mathrm{d}\theta = 0, \tag{4.6}$$

and

$$\tfrac{3}{4}A_\infty \frac{\mathrm{d}}{\mathrm{d}\tau}\oint A_{0\theta}^2\,\mathrm{d}\theta = \oint A_0\,V(A_0)\,\mathrm{d}\theta, \tag{4.7}$$

which must be satisfied to eliminate secular terms in the solution for A_1, where $\oint$ denotes an integral over one period. It can be seen from (4.5) that the first-order solution A_0 has one free parameter, the modulus-squared m. The orthogonality relations (4.6) and (4.7) cannot be satisfied simultaneously by one value of m. Hence a steady undular bore is not a solution of (4.1).

The long-term behaviour of the solution away from the forcing may be obtained

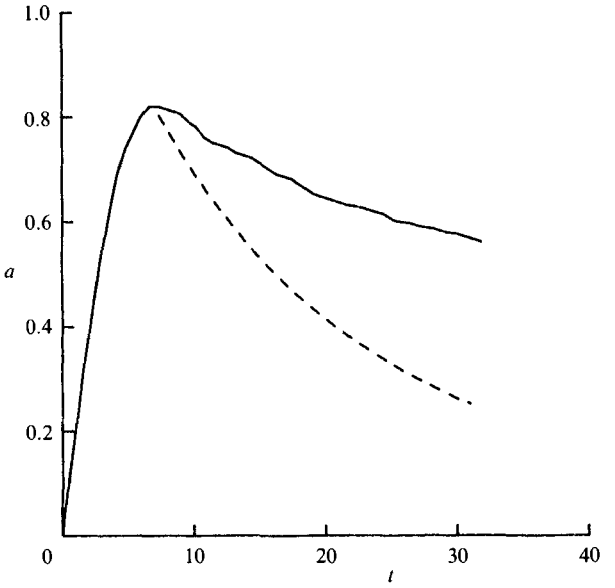

FIGURE 6. Amplitude a of the lead wave of the upstream wavetrain in figure 5(a) as a function of t (——); amplitude a of an unforced isolated soliton as a function of t (– – – –).

from the mass conservation equation for (4.1) away from the forcing. This equation yields

$$\frac{\mathrm{d}\bar{A}}{\mathrm{d}t} \propto \frac{\mathrm{d}}{\mathrm{d}t}\oint A\,\mathrm{d}x = -\delta \oint V(A)\,\mathrm{d}x. \tag{4.8}$$

The mean height of the solution away from the forcing decays and hence the long-term solution of (4.1) is a localized steady state over the forcing. The continual decay of the solution away from the forcing can be seen in the numerical solution shown in figure 5(a). This decay of the bores upstream and downstream of the forcing is due to the non-local nature of the viscous term.

As in § 3, we may again examine the amplitude behaviour of the lead wave of the upstream wavetrain. In figure 6, the amplitude of the lead wave of the upstream wavetrain in figure 5(a) is plotted as a function of t. Keulegan (1948) showed that the amplitude a of an isolated, unforced soliton decays under the action of boundary-layer friction as

$$a = a_0[1+0.1514\,a_0^{\frac{1}{2}}\delta(t-t_0)]^{-4}, \tag{4.9}$$

where a_0 is the initial amplitude of the soliton and t_0 is the initial time. This amplitude decay is also plotted in figure 6, with a_0 taken as the maximum amplitude of the lead upstream wave and t_0 the time at which this maximum is attained, as was done in § 3. We again see that the behaviour of the upstream wavetrain is not the same as a train of isolated solitons. This is again due to the upstream wavetrain being a modulated cnoidal wave whose individual waves are linked together. Also, as was the case in § 3, the damping causes the modulus of each of the waves in the wavetrain to decrease, so that the upstream wavetrain becomes increasingly less like a train of solitons as t increases.

The solution for an intermediate value of δ, $\delta = 0.3$, is shown in figure 5(b). The oscillations of the undular bore have been nearly damped out, so that the solution

	Experimental	Numerical $\delta = 0.0561$	Numerical $\delta = 0$
	(*a*) $\Delta = -2.19$, $g_0 = 4.50$		
a	1.15	1.06	1.55
A_+	−1.20	−1.30	−1.59
a_+	1.60	2.43	3.18
τ_1	0.95	1.11	1.29
τ_2	0.92	1.02	1.16
	(*b*) $\Delta = 0.120$, $g_0 = 4.50$		
a	2.22	1.85	2.50
A_+	−0.93	−0.95	−1.19
a_+	1.44	1.64	2.38
τ_1	1.23	1.13	1.29
τ_2	0.99	1.07	1.16

TABLE 2. Comparison of the experimental results of Lee (1985) and numerical results with boundary-layer friction and with no friction

consists of a mean-level variation. Away from the forcing, this mean level is slowly damped out, so that after a long time, the solution away from the forcing is zero.

Lee (1985) experimentally studied the surface waves produced by moving a two-dimensional obstacle along the bottom of a wave tank containing a shallow layer of water at a Froude number near 1. To obtain a quantitative comparison between the present numerical results and the experimental results of Lee, we find from (2.15*a*) that for these experiments, $\delta = 0.0561$ (upon using the values of the parameters given by Lee). In the present notation, the forcing used by Lee is

$$G = -18.85 + (545.3 - 1119.7\,x^2)^{\frac{1}{2}}, \quad |x| \leqslant 0.4118. \tag{4.10}$$

Two representative sets of experimental results will be compared with the solution of (4.1) with $\delta = 0.0561$. In the present notation, these experimental results correspond to (*a*) $\Delta = -2.19, g_0 = 4.50$ and (*b*) $\Delta = 0.120, g_0 = 4.50$ ($\Delta = -2.19$ and $\Delta = 0.120$ correspond to Froude numbers of 0.89 and 1.01 respectively). Table 2 presents a comparison between the amplitude a of the lead upstream wave, the level A_+ of the downstream depression, the amplitude a_+ of the trailing wave of the downstream wavetrain and the periods τ_1 and τ_2 of the first two waves of the downstream wavetrain for these values of Δ and g_0. In the table, the values of these quantities are shown for the experimental results of Lee, for the numerical results with $\delta = 0.0561$ and for the numerical results with $\delta = 0$. It can be seen that the effect of boundary-layer friction goes some way towards accounting for the difference between the experimental and theoretical results for $\delta = 0$. In the derivation of Korteweg–de Vries equations of the form (1.1) or (4.1), higher-order nonlinear and dispersive terms of $O(a^2\alpha)$ are neglected (the Korteweg–de Vries terms being $O(a\alpha^{\frac{1}{2}})$). For the experiments of Lee, $\alpha = 0.2$, so that the viscous term in (4.1) is of the same order as these neglected terms. These higher-order terms are the cause of the difference between the solutions of (4.1) and the experimental results. Since the amplitudes of the upstream waves are higher for $\Delta = 0.120$ than for $\Delta = -2.19$ and the converse is the case for the downstream waves, these higher-order terms explain why the agreement between the experimental and numerical amplitudes is better for the upstream than the downstream waves for $\Delta = -2.19$ and vice versa for $\Delta = 0.120$.

	Experimental	Numerical results of Melville & Helfrich	Numerical $\delta = 0.563$
		(*a*) $\Delta = -5.59$	
a	—	7.84	3.98
A_+	−3.10	−4.27	−4.50
a_+	4.44	8.26	7.55
		(*b*) $\Delta = 8.39$	
a	6.60	6.60	9.18
A_+	−1.86	−2.44	−2.80
a_+	2.83	4.64	3.78

TABLE 3. Comparison of experimental and numerical results of Melville & Helfrich (1987) and the solutions of (4.1)

Melville & Helfrich (1987) studied the flow produced by towing an obstacle through a two-layer fluid consisting of kerosene and water at a resonant velocity. Their experiments had $\alpha = 0.30$, so that the wave amplitudes are too large for the present weakly nonlinear theory to apply. For their numerical solutions, the authors used a forced, extended Korteweg–de Vries equation incorporating terms cubic in the nonlinearity. Even though good agreement between the solutions of (4.1) and the experimental results is not expected, a comparison is shown in table 3, where the amplitude a of the lead wave of the upstream wavetrain, the level A_+ of the downstream depression and the amplitude a_+ of the trailing wave of the downstream wavetrain for the solutions of (4.1) are compared with the numerical and experimental results of Melville & Helfrich. The forcing used by Melville & Helfrich was (2.19) with $g_0 = 74.21$ and $\xi = 5.557$. From (2.15*b*), it is found that the reported experimental data gives $\delta = 0.563$, so again δ is of the same order as the higher-order terms. The experimental results in table 3 are for Froude numbers of 0.94 and 1.09, which correspond to $\Delta = -5.59$ and $\Delta = 8.39$ respectively. Owing to the recording equipment used in the experiments, no experimental value of a for $\Delta = -5.59$ was found. It can be seen that, on the whole, the addition of viscosity to the weakly nonlinear Korteweg–de Vries model does not result in better agreement with the experimental results than the forced, extended Korteweg–de Vries equation used by Melville & Helfrich. The only improvement in agreement occurs for the amplitude a_+ of the trailing wave of the downstream wavetrain. As stated, good agreement was not expected as the amplitudes of the waves are beyond the range of validity of a first-order weakly nonlinear theory, these waves having amplitudes $O(\alpha^{\frac{1}{2}})$.

Baines (1984) conducted a similar series of experiments using a moving obstacle to resonantly force a two-layer fluid consisting of kerosene and water. In these experiments, the values of α ranged from $O(10^{-1})$ to $O(1)$, so that for many of the experimental results, higher-order terms must be included. Using (2.15*b*), it can be found from the experimental parameters that δ took values around 0.5, with the exact value depending on the depths of the two layers, which were variable in the experiments. Since the higher-order nonlinear and dispersive terms neglected in the derivation of (4.1) are $O(\alpha^{\frac{1}{2}})$ relative to the terms appearing in (4.1), we again have that these higher-order terms are of the same order as the viscous term. As for the experiments of Lee and Melville & Helfrich, viscosity explains some of the differences between the inviscid theory and the experimental results, but to fully account for the differences, higher-order nonlinear and dispersive terms must be included.

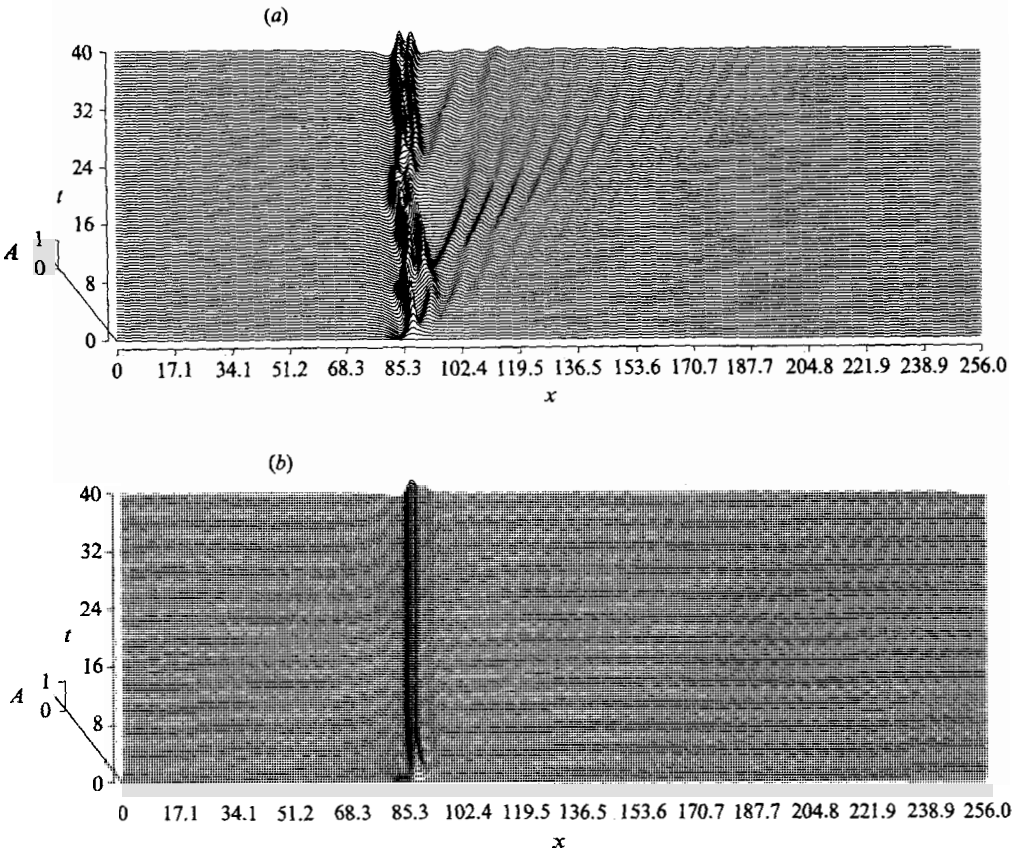

FIGURE 7. Numerical solution of (4.1) with $\Delta = 0$, $g_0 = -1$ and $\xi = 0.3$. (*a*) $\delta = 0.1$, (*b*) 1.0.

Further discussion of the effect of boundary-layer friction for small δ will be delayed until the next section, so that comparison can be made with the effect of the kinematic viscosity of the fluid as a whole.

4.2. *Positive forcing, strong damping*

The solution of (4.1) for $\Delta = 0$, $g_0 = 1$, $\xi = 0.3$ and $\delta = 1.0$ is shown in figure 5(*c*). The solution for large δ is similar to the solution for large ϵ in §3, in that a localized steady state forms over the forcing with the solution zero elsewhere. This steady state results from a balance between the forcing and the dissipation.

4.3. *Negative forcing, weak damping*

An example of the solution for negative forcing and weak damping is shown in figure 7(*a*), where $\Delta = 0$, $g_0 = -1$, $\xi = 0.3$ and $\delta = 0.1$. For comparison, the solution for $\delta = 0$ is shown in figure 1(*b*). It can be seen that the solution for negative forcing is similar to that for the increasing-depth case of §3. Small values of the damping leave the solution over the forcing unsteady. The damping for $\delta = 0.1$ is sufficiently large to damp out any waves that propagate upstream in the solution for $\delta = 0$.

4.4. *Negative forcing, strong damping*

An example of the solution for strong damping and negative forcing is shown in figure 7(*b*), where the numerical solution is for $\Delta = 0$, $g_0 = -1$, $\xi = 0.3$ and $\delta = 1.0$.

Again strong damping results in the formation of a localized steady state over the forcing, this steady state resulting from a balance between dissipation and forcing.

5. Forced Korteweg–de Vries–Burgers' equation

The final type of dissipation to be considered in the present work is that due to the viscosity of the fluid as a whole. As stated in §4, in experimental and physical situations, this type of viscous force will usually be less important than that due to the action of viscosity in boundary layers and/or interfaces. For example, for the experiments of Lee (1985), it can be found from (2.15a) and (2.18) that $\nu = 1.27 \times 10^{-4}$, while $\delta = 0.0561$. However, the simpler form of the viscous term compared with the viscous term for the case of boundary-layer viscosity allows the analysis to proceed further. The present form of the dependence on viscosity provides a contrast to the situation for boundary-layer viscosity in that a steady undular bore ultimately forms upstream and downstream of the forcing, whereas for boundary-layer viscosity, the undular bores upstream and downstream of the forcing are unsteady and decay to zero.

The forced Korteweg–de Vries equation incorporating viscosity is the forced KdV–Burgers' equation

$$-A_t - \Delta A_x + 6AA_x + A_{xxx} + G_x + \nu A_{xx} = 0. \tag{5.1}$$

Let us first consider the case of positive forcing.

5.1. *Positive forcing, weak damping*

Figure 8(a) shows the numerical solution of (5.1) for $\Delta = 0, \nu = 0.1$ and the forcing (2.19) with $g_0 = 1$ and $\xi = 0.3$. The corresponding solution for $\nu = 0$ is shown in figure 1(a) and the solution for the corresponding value of boundary-layer viscosity is shown in figure 5(a). Small values of viscosity for both the present dissipation and that of §4 lead to the formation of undular bores upstream and downstream of the forcing. These bores occur because a constant is a solution of (4.1) and (5.1), as explained in §4.

The jump in height across the upstream and downstream bores is greater for the present case than for the boundary-layer viscosity case. The reason for this can be found by considering the mass conservation equations for (4.1) and (5.1), which are

$$-\frac{\partial}{\partial t}(A) + \frac{\partial}{\partial x}(-\Delta A + 3A^2 + A_{xx} + G) - \delta V(A) = 0 \tag{5.2}$$

and

$$-\frac{\partial}{\partial t}(A) + \frac{\partial}{\partial x}(-\Delta A + 3A^2 + A_{xx} + G + \nu A_x) = 0 \tag{5.3}$$

respectively. From these equations, we obtain

$$\frac{\mathrm{d}\bar{A}}{\mathrm{d}t} \propto \frac{\mathrm{d}}{\mathrm{d}t} \oint A \, \mathrm{d}x = -\delta \oint V(A) \, \mathrm{d}x \tag{5.4}$$

and

$$\frac{\mathrm{d}\bar{A}}{\mathrm{d}t} \propto \frac{\mathrm{d}}{\mathrm{d}t} \oint A \, \mathrm{d}x = 0 \tag{5.5}$$

for (4.1) and (5.1) respectively, where $\oint$ denotes that the integral is taken over one period. Therefore mean height is conserved in the present case, but is not in the boundary-layer-friction case. The jump across the undular bore will therefore be less

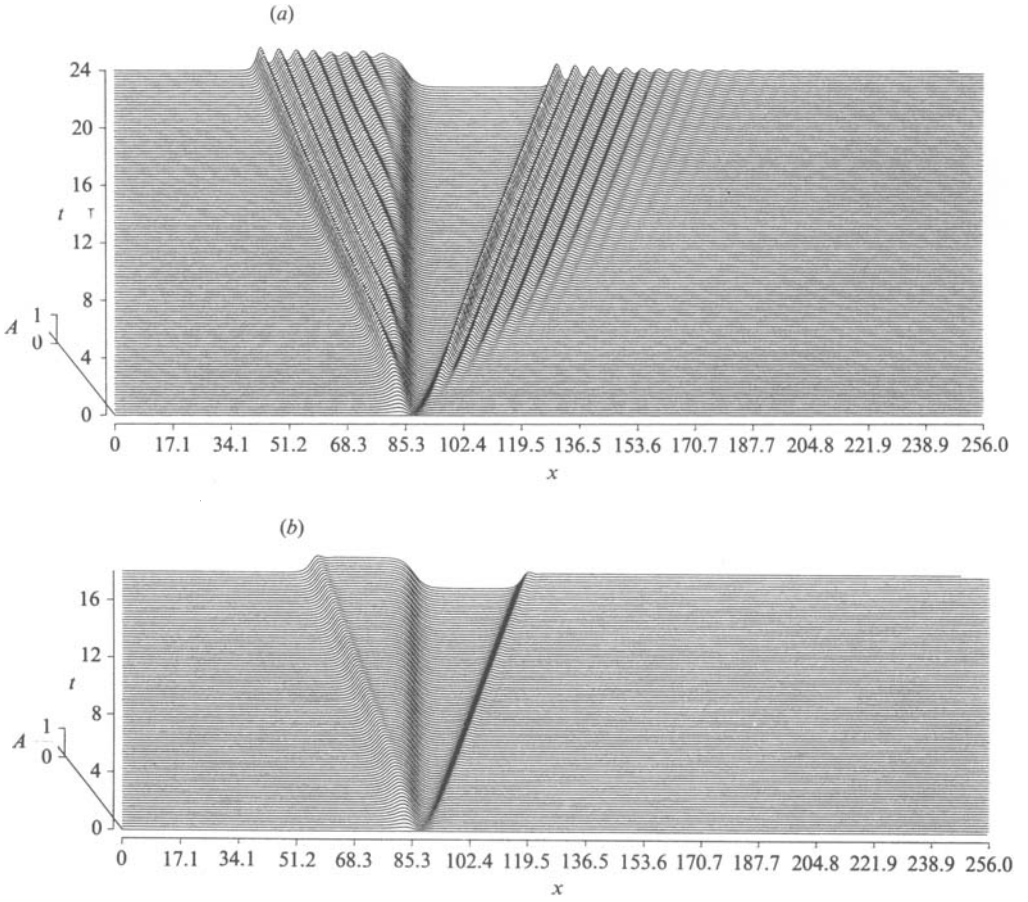

FIGURE 8. Numerical solution of (5.1) with $\Delta = 0$, $g_0 = 1$ and $\xi = 0.3$. (*a*) $\nu = 0.1$, (*b*) 1.0.

in the case of boundary-layer viscosity. It can be seen that (5.5) implies that, in the present case, the undular bore can become steady and the long-term solution will be a drop in level across the forcing, in contrast to the situation in the case of boundary-layer viscosity, where the undular bore is unsteady and the solution away from the forcing decays to zero.

It can be seen on comparison of figures 1(*a*), 5 (*a*) and 8(*a*) that, at a given time t, small values of ν result in the length of the downstream depression increasing, whereas small values of δ for boundary-layer friction leave this length relatively unchanged. The reason for this can be found from the expression (3.2) for the phase speed of a cnoidal wave. In the present case, the mean level $\bar{A}$ remains largely unchanged from its value for $\nu = 0$ and the amplitude a of the cnoidal waves is reduced. Hence c increases, so that the length of the downstream depression increases. In the case of boundary-layer viscosity, both $|\bar{A}|$ ($\bar{A} < 0$) and a decrease. These two changes have opposite effects and, from the numerical solution, we see that they nearly balance each other.

Upon closer examination of the solution for small ν shown in figure 8(*a*), it can be seen that initially the solution for small ν behaves like the solution for $\nu = 0$ shown in figure 1(*a*). As time increases, each wave crest then decreases in amplitude until

a steady value is reached. Johnson (1970) found the steady undular-bore solution of (5.1) for small ν. This solution is

$$A = b_-(\tau) + a_-(\tau)\,\mathrm{cn}^2\,\alpha_-(\tau)\,\theta, \tag{5.6}$$

where

$$\left.\begin{aligned} &\theta = \tfrac{1}{2}(3A_\infty^-)^{\frac{1}{2}}[x + (3A_\infty^- - \Delta)\,t]; \\ &\tau = \frac{2\nu\theta}{(3A_\infty^-)^{\frac{1}{2}}} = \nu[x + (3A_\infty^- - \Delta)\,t], \\ &b_- = \tfrac{1}{2}A_\infty^- - \frac{a_-}{3m}(2m-1), \quad a_- = \tfrac{3}{2}A_\infty^- m(m^2-m+1)^{-\frac{1}{2}}, \quad \alpha_- = \left(\frac{2a_-}{3m}\right)^{\frac{1}{2}} \end{aligned}\right\} \tag{5.7}$$

and

$$A_-\,\mathrm{e}^{-\tau} = (m^2-m+1)^{-\frac{5}{4}}[(m^2-m+1)\,E(m) - \tfrac{1}{2}(1-m)\,(2-m)\,K(m)]. \tag{5.8}$$

E and K are complete elliptic integrals of the first and second kind respectively of modulus-squared m, A_∞^- is the value of A resulting from the passage of the bore and A_- is a constant. As $t \to \infty$, the solution on the entire upstream side of the forcing approaches A_∞^-.

For small ν, the solution of (5.1) then behaves essentially as the non-viscous solution of Smyth (1987), then, under the action of viscosity, evolves into the undular bore given by (5.6)–(5.8). To evaluate the constant A_- in (5.8), we may take the undular bore as developing from a train of solitons. The solution never attains the fully developed modulated cnoidal wave solution for $\nu = 0$ but, for small ν, taking the undular bore as developing from an initial soliton wavetrain is a good approximation. Therefore the constant A_- is approximately

$$A_- = \mathrm{e}^{\tau_0}, \tag{5.9}$$

where τ_0 is the value of τ at the time at which the undular bore first starts to form. For the solution shown in figure 8(*a*),

$$\tau_0 \approx \nu[66.0 + 33\,A_\infty^-]. \tag{5.10}$$

Since the passage of the bore results in the formation of a steady state, the solution of (5.1) for large time is the solution of

$$-\Delta A_x + 6AA_x + A_{xxx} + G_x + \nu A_{xx} = 0. \tag{5.11}$$

From GS, it can then be shown that

$$A_\infty^- = \tfrac{1}{6}[\Delta + (12g_0)^{\frac{1}{2}}] + O(\nu). \tag{5.12}$$

For $\Delta = 0$ and $g_0 = 1, A_\infty^- = 0.577 + O(\nu)$, which compares well with the numerical value of $A_\infty^- = 0.56$.

The wave at the head of the undular bore (5.6) has $m = 1$ and so is a solitary wave. From (5.7), we find that the amplitude of this wave is given by

$$a_\mathrm{s} = \tfrac{3}{2}A_\infty^-. \tag{5.13}$$

Using (5.12), we find that for $\Delta = 0$ and $g_0 = 1, a_\mathrm{s} = 0.87$, which compares well with the numerical value $a_\mathrm{s} = 0.82$. For small ν, the undular bore given by (5.6)–(5.8) and (5.12) is then in good agreement with the numerical solution.

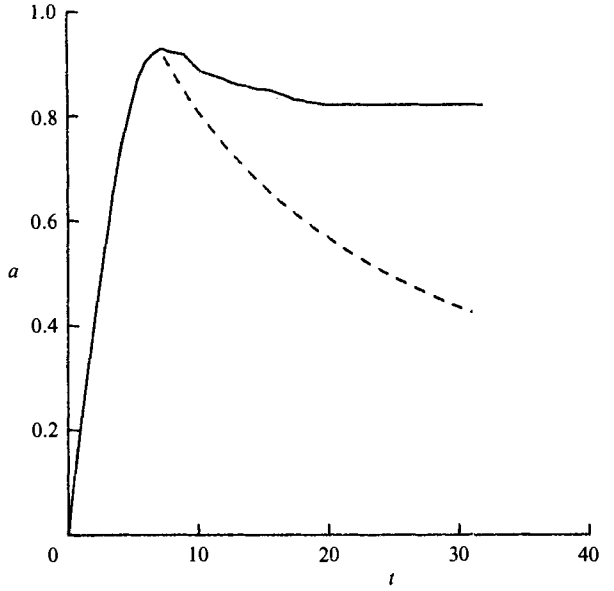

FIGURE 9. Amplitude a of the lead wave of the upstream wavetrain in figure 8(a) as a function of t (——); amplitude a of an unforced isolated soliton as a function of t (– – – –).

In figure 9, the amplitude a of the lead upstream wave in figure 8(a) is plotted as a function of time. Karpman (1979) showed that the amplitude a of the soliton solution of (5.1) for $G = 0$ decays as

$$a = a_0[1 + \tfrac{8}{15}a_0\,\nu(t-t_0)]^{-1}, \tag{5.14}$$

where a_0 is the initial amplitude of the soliton and t_0 the initial time. This amplitude decay is also plotted in figure 9 with a_0 and t_0 chosen as in § 3, i.e. a_0 is taken as the maximum amplitude of the lead upstream wave and t_0 the time at which this maximum is attained. The development of the lead upstream wave into a wave of constant amplitude can be clearly seen. The behaviour of a single isolated soliton and the waves of the upstream wavetrain under the present viscous force are distinctly different, as was the case in §§ 3 and 4. This difference is again due to the fact that the upstream wavetrain is a modulated cnoidal wave whose individual waves are linked together and, through this linkage, are linked to the forcing. This linkage results in a steady undular bore being able to form upstream of the forcing. If the upstream wavetrain were a series of isolated solitons, (5.14) shows that the wavetrain would decay to zero. So again, while it is useful to consider the upstream wavetrain as a series of solitons for qualitative purposes, the full modulated cnoidal wave character must be taken into account for quantitative purposes.

The solution downstream of the forcing behaves in a similar manner to that upstream. For small times, the solution behaves as the modulated cnoidal wavetrain of GS and Smyth (1987). This solution then evolves into the undular bore of Johnson (1970). For small ν, this undular bore is

$$A = b_+(\tau) + a_+(\tau)\,\mathrm{cn}^2\,\alpha_+(\tau)\,\theta, \tag{5.15}$$

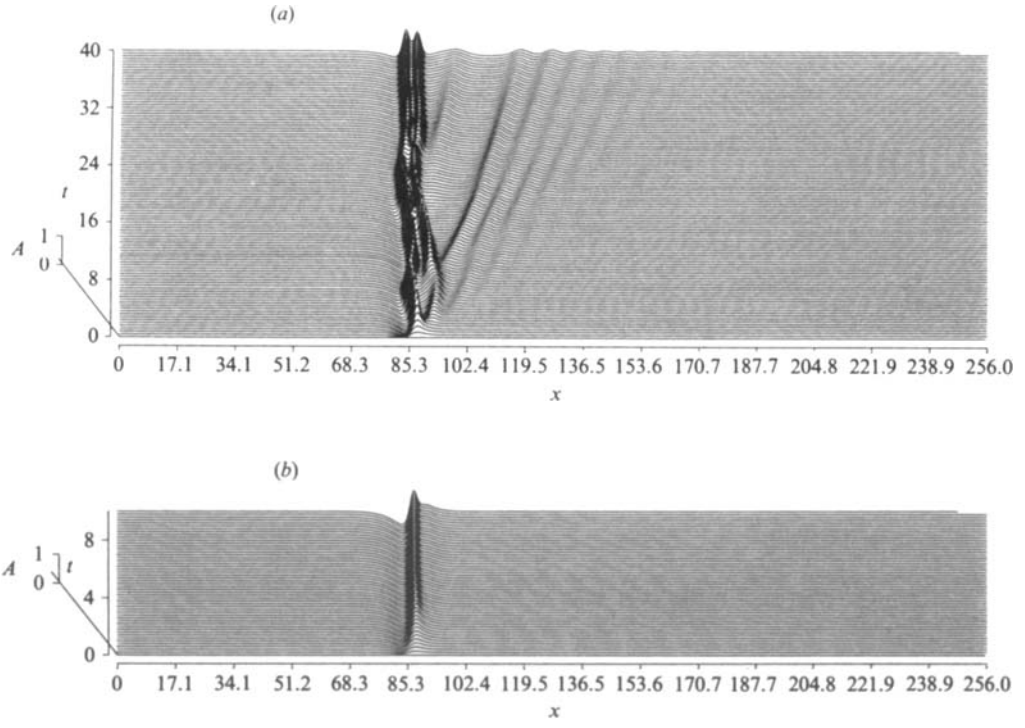

FIGURE 10. Numerical solution of (5.1) with $\Delta = 0$, $g_0 = -1$ and $\xi = 0.3$. (*a*) $\nu = 0.1$, (*b*) 1.0.

where

$$\left.\begin{aligned} \theta &= \tfrac{1}{2}(3|A_\infty^+|)^{\frac{1}{2}}[x+(3A_\infty^+-\Delta)t], \quad \tau = \nu[x+(3A_\infty^+-\Delta)t], \\ b_+ &= \tfrac{1}{2}A_\infty^+ - \frac{a_+}{3m}(2m-1), \quad a_+ = \tfrac{3}{2}m|A_\infty^+|\,(m^2-m+1)^{-\frac{1}{2}}, \quad \alpha_+ = \left(\frac{2a_+}{3m}\right)^{\frac{1}{2}}, \\ A_+\,\mathrm{e}^{-\tau} &= (m^2-m+1)^{-\frac{5}{4}}[(m^2-m+1)\,E(m)-\tfrac{1}{2}(1-m)\,(2-m)\,K(m)]. \end{aligned}\right\} \tag{5.16}$$

It can be shown from GS that

$$A_\infty^+ = \tfrac{1}{6}[\Delta-(12g_0)^{\frac{1}{3}}]+O(\nu). \tag{5.17}$$

From (5.16), we have that the amplitude of the trailing soliton of the bore is given by

$$a_s = \tfrac{3}{2}|A_\infty^+|. \tag{5.18}$$

For the solution shown in figure 8(*a*), the numerical values of A_∞^+ and a_s are -0.572 and 0.86 respectively, which compare well with the theoretical values of -0.577 and 0.866.

5.2. *Positive forcing, strong damping*

The numerical solution of (5.1) for $\Delta = 0$, $g_0 = 1$, $\xi = 0.3$ and $\nu = 1.0$ is shown in figure 8(*b*). It can be seen from figures 5(*c*) and 8(*b*) that the strong-damping solutions for the present case and the boundary-layer viscosity of §4 are very different. In the case of boundary-layer viscosity, a localized steady state develops over the forcing, while for the present case, bores propagate upstream and

downstream of the forcing. While the mass conservation results (5.4) and (5.5) strictly apply only for small values of δ and ν, they can be used to give an explanation for the observed differences in the solutions for large δ and ν. The mass conservation results show that the mean level for the case of boundary-layer viscosity will rapidly decay to zero, which precludes the permanent formation of a bore. However, for the present case, the mean level is conserved, so that a bore can form. In the case of large values of ν, the oscillations of the undular bore are completely damped out and the solution consists of a mean-level variation only.

Using a phase-plane analysis, Johnson (1970) found that an undular bore occurs for $\nu \leqslant 2(3|A_\infty|)^{\frac{1}{2}}$. For $\nu > 2(3|A_\infty|)^{\frac{1}{2}}$, the solution is a monotonic profile resulting from the dominance of the dissipative terms in (5.1). This monotonic profile is then basically a smoothed-out hydraulic jump. The critical value $2(3|A_\infty|)^{\frac{1}{2}}$ of ν has the value 2.63 for $\Delta = 0$ and $g_0 = 1$ (on using (5.7) or (5.16)). The solution shown in figure 8(*b*) has ν sufficiently close to this critical value for most of the oscillations of the undular bore to be absent.

5.3. *Negative forcing, weak damping*

The solution for negative forcing is similar to that for the boundary-layer viscosity of § 4. The solution for $g_0 = -1$, $\xi = 0.3$, $\Delta = 0$ and $\nu = 0.1$ is shown in figure 10(*a*). This can be compared with the solution for weak boundary-layer friction shown in figure 7(*a*) and the solution for $\nu = 0$ shown in figure 1(*b*). Small values of ν result in the solution over the forcing remaining unsteady.

5.4. *Negative forcing, strong damping*

Figure 10(*b*) shows the solution of (5.1) for $\Delta = 0$, $g_0 = -1$, $\xi = 0.3$ and $\nu = 1.0$. This solution may be compared with the boundary-layer-viscosity solution for $\delta = 1.0$ shown in figure 7(*b*) and the solution for $\nu = 0$ shown in figure 1(*b*). Large values of ν result in the formation of an isolated steady state over the forcing, as was the case for large values of δ in § 4. This steady state is again the result of a balance between forcing and dissipation.

The author wishes to acknowledge support from the Australian Research Grants Scheme under Grant 83/15835.

REFERENCES

AKYLAS, T. R. 1984 On the excitation of long nonlinear water waves by a moving pressure distribution. *J. Fluid Mech.* **141**, 455–466.

BAINES, P. G. 1984 A unified description of two-layer flow over topography. *J. Fluid Mech.* **146**, 127–167.

COLE, S. L. 1985 Transient waves produced by flow past a bump. *Wave Motion* **7**, 579–587.

FORNBERG, B. & WHITHAM, G. B. 1978 A numerical and theoretical study of certain nonlinear wave phenomena. *Phil. Trans. R. Soc. Lond.* A **289**, 373–404.

GRIMSHAW, R. H. J. 1983 Solitary waves in density stratified fluids. In *Nonlinear Deformation Waves, IUTAM Symp., Tallinn 1982* (ed. U. Nigul & J. Engelbrecht), pp. 431–447. Springer.

GRIMSHAW, R. H. J. & SMYTH, N. F. 1986 Resonant flow of a stratified fluid over topography. *J. Fluid Mech.* **169**, 429–464.

HAMMACK, J. L. & SEGUR, H. 1974 The Korteweg–de Vries equation and water waves. Part 2. Comparison with experiments. *J. Fluid Mech.* **65**, 289–314.

JOHNSON, R. S. 1970 A nonlinear equation incorporating damping and dispersion. *J. Fluid Mech.* **42**, 49–60.

KARPMAN, V. I. 1979 Soliton evolution in the presence of perturbation. *Physica Scr.* **20**, 462–478.

KEULEGAN, G. H. 1948 Gradual damping of solitary waves. *J. Res. Natn. Bur. Stand.* **40**, 487–498.

KNICKERBOCKER, C. J. & NEWELL, A. C. 1980 Shelves and the Korteweg–de Vries equation. *J. Fluid Mech.* **98**, 803–818.

LEE, S.-J. 1985 Generation of long water waves by moving disturbances. Ph.D. thesis, California Institute of Technology.

LEONE, C., SEGUR, H. & HAMMACK, J. L. 1982 Viscous decay of long internal solitary waves. *Phys. Fluids* **25**, 942–944.

MELVILLE, W. K. & HELFRICH, K. R. 1987 Transcritical two-layer flow over topography. *J. Fluid Mech.* **178**, 31–52.

MILES, J. W. 1976 Korteweg–de Vries equation modified by viscosity. *Phys. Fluids* **19**, 1063.

OVSTROVSKY, L. A. 1976 Short-wave asymptotics for weak shock waves and solitons in mechanics. *Intl J. Nonlinear Mech.* **11**, 401–416.

SMYTH, N. F. 1987 Modulation theory solution for resonant flow over topography. *Proc. R. Soc. Lond.* A **409**, 79–97.

WEIDMAN, P. & MAXWORTHY, T. 1978 Experiments on strong interactions between solitary waves. *J. Fluid Mech.* **85**, 417–431.

WHITHAM, G. B. 1974 *Linear and Nonlinear Waves*. Wiley.